⌘ *Author's Choice*

THE JOURNAL OF BIOLOGICAL CHEMISTRY VOL. 288, NO. 3, pp. 1511–1520, January 18, 2013
Published in the U.S.A.

The Maturational Refolding of the β-Hairpin Motif of Equine Infectious Anemia Virus Capsid Protein Extends Its Helix α1 at Capsid Assembly Locus*[S]

Received for publication, October 3, 2012, and in revised form, November 19, 2012 Published, JBC Papers in Press, November 26, 2012, DOI 10.1074/jbc.M112.425140

Kang Chen[‡], **Grzegorz Piszczek**[§], **Carol Carter**[¶1], **and Nico Tjandra**[‡2]

From the [‡]*Laboratory of Molecular Biophysics and* [§]*Biophysics Facility, NHLBI, National Institutes of Health, Bethesda, Maryland 20892 and the* [¶]*Department of Molecular Genetics & Microbiology, Stony Brook University, Stony Brook, New York 11794*

Background: The function of the maturational refolded N-terminal β-hairpin in retroviral capsid remains unknown.
Results: Folding the β-hairpin of equine infectious anemia virus (EIAV) capsid extends its downstream helix α1 at the N terminus, which forms the oligomerization core of retroviral capsids.
Conclusion: The β-hairpin structures helix α1, which could be necessary for capsid assembly.
Significance: Solution NMR revealed the function of the puzzling β-hairpin motif in retroviral capsid.

A retroviral capsid (CA) protein consists of two helical domains, CA^N and CA^C, which drive hexamer and dimer formations, respectively, to form a capsid lattice. The N-terminal 13 residues of CA refold to a β-hairpin motif upon processing from its precursor polyprotein Gag. The β-hairpin is essential for correct CA assembly but unexpectedly it is not within any CA oligomeric interfaces. To understand the β-hairpin function we studied the full-length CA protein from equine infectious anemia virus (EIAV), a lentivirus sharing the same cone-shaped capsid core as HIV-1. Solution NMR spectroscopy is perfectly suited to study EIAV-CA that dimerizes weaker than HIV-1-CA. Comparison between the wild-type (wt) EIAV-CA and a variant lacking the β-hairpin structure demonstrated that folding of the β-hairpin specifically extended the N terminus of helix α1 from Tyr^{20} to Pro^{17}. This coil to helix transition involves the conserved sequence of Thr^{16}-Pro^{17}-Arg^{18} (Ser^{16}-Pro^{17}-Arg^{18} in HIV-1-CA). The extended region of helix α1 constituted an expanded EIAV-CA^N oligomeric interface and overlapped with the HIV-1-CA hexamer-core residue Arg^{18}, helical in structure and pivotal in assembly. Therefore we propose the function of the maturational refolding of the β-hairpin in CA assembly is to extend helix α1 at the N terminus to enhance the CA^N oligomerization along the capsid assembly core interface. In addition, NMR resonance line broadening indicated the presence of micro-millisecond exchange kinetics due to the EIAV-CA^N domain oligomerization, independent to the faster EIAV-CA^C domain dimerization.

Viruses in the family Retroviridae, *e.g.* human immunodeficiency virus (HIV), simian immunodeficiency virus, avian sarcoma virus, and equine infectious anemia virus (EIAV),[3] utilize reverse transcription to replicate the genetic information stored in their RNA genome (1). Mutational analyses indicate that the viral capsid plays a critical role in this event because even small structural changes can disrupt the process (2–8). A retrovirion cycles through morphological transitions: viral particle assembly, budding, and maturation occurs in producer cells; the particle is disassembled in the newly infected target cell. At the onset of HIV-1 assembly, the structural precursor polyprotein, Gag, assembles underneath the plasma membrane (9–11). During or after budding, maturational changes proceed wherein the full-length Gag proteins in the assemblages are cleaved by viral-encoded protease (PR) to generate three major products, matrix (MA), capsid (CA), and nucleocapsid (NC). These are arranged to comprise a MA shell underlying the lipid envelope and a conical (*e.g.* HIV-1, simian immunodeficiency virus, EIAV, *i.e.* lentivirus subgroup) or spherical (*e.g.* avian sarcoma virus) CA core that encapsulates the genome, which is bound to NC (12–14). For all retroviruses the N-terminal 12–13 residues of CA, unstructured within Gag, refold into a β-hairpin structural motif stabilized by a Pro^1-Asp^{51} (HIV-1) salt bridge (2). The salt bridge involving the conserved residue proline 1 is essential and any mutations affecting salt bridge stability will unfold the β-hairpin and cause defects in the assembled capsid that eventually result in noninfectious virions (2–7). Correct assemblage of native CA proteins during viral maturation ensures protection and integrity of the packaged viral genome. After virion entry into another host cell, the capsid disassembles to allow its genomic RNA to be released and reverse transcribed. This step requires the structural integrity and correct assembly of CA proteins (15, 16).

Successful viral maturation therefore depends on folding of the β-hairpin motif and the reversible quaternary packing of CA proteins. A retroviral CA protein consists of two helical domains, the 17-kDa N-terminal (CA^N) and the 9-kDa C-ter-

* This work was supported, in whole or in part, by the National Institutes of Health Intramural Research Program of NHLBI.
⌘ *Author's Choice*—Final version full access.
[S] This article contains supplemental "Experimental Procedures," "Results," and Fig. S1.
[1] To whom correspondence may be addressed. Tel.: 631-632-8801; Fax: 631-632-9797; E-mail: ccarter@ms.cc.sunysb.edu.
[2] To whom correspondence may be addressed. Tel.: 301-402-3029; Fax: 301-402-3405; E-mail: tjandran@nhlbi.nih.gov.

[3] The abbreviations used are: EIAV, equine infectious anemia virus; RDC, residual dipolar coupling; MA, matrix; CA, capsid; NC, nucleocapsid; PDB, Protein Data Bank; S, Svedberg sedimentation coefficient unit; TROSY, transverse relaxation optimized spectroscopy.

minal domains (CA^C). For HIV-1, the wild-type (wt) CA protein exists in solution mainly as dimers and some minor amount of other oligomers (17–21). High-resolution structures have been obtained for the individual retroviral CA domains (22–29) and the monomeric full-length CA (30–33). Interestingly, the sizes, secondary, and tertiary structures of different CA proteins are highly conserved (34). The hexagonal and pentagonal assembly (35, 36) of the full-length CA through CA^N domains was revealed by cryoelectron microscopy (EM) and crystallography (37–42). Further dimer or trimer formation of CA^C domains connects hexamers and pentamers (38, 41). Unexpectedly, the β-hairpin motif does not form any inter-molecular contacts within high resolution CA quaternary structures.

To understand the contribution of the β-hairpin motif to CA assembly, we applied solution NMR spectroscopy to study the CA protein from EIAV, a lentivirus sharing the similar conical capsid core (12) and assembly (43) structure as HIV-1. Different from HIV-1-CA, EIAV-CA dimerizes much weaker in solution, which results in sharper NMR resonance peaks and is more suitable for study by solution NMR. Previous results on HIV-1-CA showed that any point mutation, deletion mutation, or N-terminal extension at Pro^1 would affect the Pro^1-Asp^{51} salt bridge and unfold the β-hairpin (2). The published crystal structure of EIAV-CA is an N-terminal 3-residue (Pro^1-Met^3) deletion mutant with an unfolded signature β-hairpin (44). Instead of using this deletion mutant, which lacks resonances from residues Pro^1 to Met^3, we studied a N-terminal histidine-tagged variant that could also unfold the β-hairpin structure, in addition to the wt full-length EIAV-CA, to identify the structural differences associated with the β-hairpin formation. Our results showed that the maturational refolded β-hairpin induces a coil-helix transition in residues N-terminal to helix α1, Pro^{17}-Gly^{19}. The same region was also identified to be the expanded interface for the sparse CA^N domain oligomerization. The Thr^{16}-Gly^{19} sequence is highly conserved in HIV-1-CA as well, and Arg^{18} of HIV-1-CA has been demonstrated to be essential (45) and form the inner-core of the CA^N hexamer (38). Therefore we propose the function of refolding the β-hairpin, the prerequisite event for retroviral CA assembly, is to extend helix α1 at the N terminus to enhance CA^N oligomerization for assembly. Our data further suggested the CA^N oligomerization is kinetically slower and uncorrelated to the faster domain CA^C dimerization, previously not known in retroviral capsid assembly events (46).

EXPERIMENTAL PROCEDURES

Protein Purifications—The wt EIAV-CA protein consists of 230 residues and starts with proline (Fig. 1*A*). The cDNA encoding the protein was inserted upstream of the intein gene in the pTXB1 vector from New England Biolabs (Ipswich, MA). The EIAV-CA-pTXB1 construct was transformed into *Escherichia coli* host strain BL21-DE3. The EIAV-CA-intein fusion protein sequence and the DTT-induced cleavage site can be found in supplemental "Experimental Procedures" and "Results". The cells were grown in LB medium at 37 °C to an A_{600} of 0.7 and induced with 0.5 mM isopropyl 1-thio-β-D-galactopyranoside. The expression went on for another 5 h. The *E. coli* cells were pelleted from a 4-liter culture, dissolved in 500 ml of lysis buffer (20 mM Tris, pH 8, 500 mM NaCl, and 1 mM EDTA), and then passed twice through a high-pressure homogenizer, EmulsiFlex-C3 from Avestin (Ottawa, Canada). The cell lysate was centrifuged for 1 h at 35,000 × *g*. The supernatant containing the CA-intein fusion proteins was loaded onto a 20-ml gravity column filled with chitin beads (New England Biolabs). The column was then flushed with 60 ml of lysis buffer supplemented with 50 mM DTT. The on-column thiol-induced cleavage took 2 days. The CA proteins were finally eluted and dialyzed into a low-salt buffer (20 mM Tris, pH 9, and 5 mM NaCl). All of the above purification steps were performed at 4 °C. Further purifications were performed on pre-packed FPLC anion exchange (Fast-flow DEAE) and gel filtration columns (Hi-Load Superdex-75) from GE Healthcare. The identity of the purified proteins was confirmed using LC-MS. The measured molecular mass of 26075.8 Da is close to the theoretical value of 26076.9 Da. Isoelectric focusing (IEF) kits from Invitrogen were used to characterize the purified CA proteins. For NMR studies, $^2H/^{15}N/^{13}C$ triple-labeled or $^2H/^{15}N$ double-labeled CA proteins were expressed overnight at 30 °C in *E. coli* cells grown in 99.8% ^2H_2O prepared M9 minimal medium. $^{15}NH_4Cl$ and [^{13}C]glucose were the sole nitrogen and carbon sources, respectively. All isotopes were from Cambridge Isotope Laboratories (Andover, MA).

In addition to the wt EIAV-CA, another construct expressing a N-terminal histidine-tagged EIAV-CA was cloned, which had extra amino acid residues of AHHHHHHG added onto the native EIAV-CA N-terminal sequence. The full sequence of the variant can be found in supplemental "Experimental Procedures" and "Results". The variant His-EIAV-CA protein was purified using a nickel-agarose gravity column first followed by FPLC columns similar to those used for purification of the wt EIAV-CA. The isotope labeling and backbone resonance assignments were obtained as described for the wt protein.

NMR Spectroscopy and Resonance Assignment—A 0.15 mM $^2H/^{15}N/^{13}C$ triple-labeled EIAV-CA sample was used for resonance assignment. The same buffer of 20 mM potassium P_i at pH 6.7, 0.01% NaN_3, and 7% ^2H_2O was used in nearly all NMR experiments. The protein concentration was measured using its UV absorbance in 6 M guanidinium HCl (ϵ_{280} = 22460 M^{-1} cm^{-1}). Temperature for all NMR experiments was 27 °C. The backbone resonance assignments were obtained from transverse relaxation optimized spectroscopy (TROSY) (47, 48) version of three-dimensional experiments HNCO (49), HN(CA)CO (50), HNCACB, and HN(CO)CACB (51). The through space three-dimensional experiments of NOESY-TROSY-HSQC (52) and HMQC-NOE-TROSY-HSQC (in house written) were collected with a NOE mixing time of 150 ms. All data were collected on Bruker Avance 600, 800, and 900 spectrometers equipped with cryogenic probes and *Z*-axis pulse field gradients. Chemical shifts were externally referenced. The TROSY-measured amide ^{15}N and ^1H chemical shifts were offset to true chemical shift values by $^1J_{N\text{-}H}/2$. High resolution TROSY spectra, which contained 512 complex points on ^{15}N dimension, were collected on four $^{15}N/^2H$-labeled samples at concentrations ranging from 0.05 to 0.4 mM on a 900 MHz spectrometer. All NMR spectra were processed and analyzed using NMRPipe (53) and SPARKY 3 (T. D. Goddard

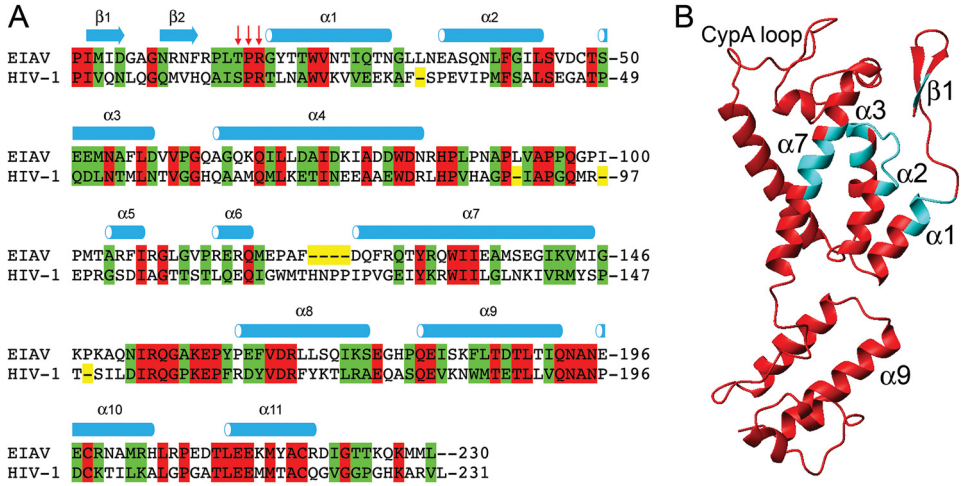

FIGURE 1. **The sequence and structure of wt EIAV-CA.** *A*, the structure based sequence alignment between EIAV-CA (UniProt ID P69732) and HIV-1-CA (UniProt ID P12497). The CA^N and CA^C domains were separately aligned according to their three-dimensional structures (77). The crystal structure coordinates of EIAV-CA (PDB code 2EIA)(44), and HIV-1-CA^N (PDB code 1AK4 or 1GWP)(23, 27) and HIV-1-CA^C (PDB code 1A43)(78) were used. Identical and homologous residues were highlighted in *red* and *green*, respectively. The *red arrows* point to the conserved sequence affected by the β-hairpin formation identified in this study. *B*, the three-dimensional structure of EIAV-CA with the refined CA^N domain possessing the β-hairpin. The *cyan* colored ribbons correspond to un-assigned residues with severe ^1H-^{15}N resonance line broadening.

and D. G. Kneller, University of California San Francisco), respectively. In-house written MATLAB (The Mathworks, MA) programs using the Simplex search algorithm were used to fit all NMR data with appropriate models. The chemical shift assignments of the wt and histidine-tagged variant EIAV-CA have been deposited into the Biological Magnetic Resonance Bank (BMRB) data base with entry numbers 18421 and 18815, respectively.

Residual Dipolar Coupling and Structure Refinement—Both high resolution TROSY and HSQC spectra were collected on samples of the $^{15}N/^{2}H$-labeled wt or variant EIAV-CA proteins on a 900 MHz NMR spectrometer. The differences in peak locations along the ^{15}N dimensions of the two spectra yielded half of the $^1J_{NH}$ coupling constants. Repeating the same measurements on the sample with an added 5–10 mg/ml of *Pf*-1 phage co-solvent (54) (ASLA Biotech) yielded summed coupling constants $(^1J_{N\text{-}H} + D_{N\text{-}H})/2$, where $D_{N\text{-}H}$ is the residual dipolar coupling (RDC) of N-H bonds. Subtraction and doubling yielded measured $D_{N\text{-}H}$ and experimental errors were taken from duplication reproducibility. A set of five alignment tensor parameters, alignment order D_a, rhombicity R, and Euler angles α, β, and γ, were used to fit measured $D_{N\text{-}H}$ to domain structural coordinates. The Q factor was calculated to check the agreement between crystal structure coordinates and $D_{N\text{-}H}$ measured in solution.

The refinement of the CA^N backbone structure included adding coordinates for missing residues and simulated annealing using XPLOR-NIH (55). In addition to force-field-related restraints within XPLOR-NIH (56), specific restraints are 90 RDCs, 155 amide ^1H-^1H NOEs, 226 Φ/Ψ dihedral angles derived from TALOS-plus (57), 85 empirical H-bond restraints, and root mean square deviation penalties for deviation away from helical residue coordinates of the original crystal structure. The structure with the lowest energy out of 500 calculated structures was chosen to model the EIAV-CA quaternary structure.

Analytical Ultracentrifugation and Data Analysis—Sedimentation velocity experiments were performed on the wt EIAV-CA protein at 0.4 mM concentrations and pH values of 4, 6, and 8. Buffer components were 100 mM NaCl for all pH values, and 20 mM NaAc for pH 4, 20 mM KPi for pH 6, and Tris-HCl for pH 8 (20 mM). A Beckman Optima XL-I analytical ultracentrifuge and a four-place AN-Ti rotor were used. Samples of 0.4 mM protein concentration were used. Centrifuge cells fitted with double-sector centerpieces and sapphire windows were filled with 0.4 ml of the protein sample and the dialysate buffer reference. After reaching thermal equilibrium at 20.0 °C at rest, the rotor was accelerated to 50,000 rpm. Interference and absorbance scans at 297 nm were started immediately after the rotor reached the set speed and collected until no further sedimentation boundary movement was observed. The apparent sedimentation coefficient distributions were analyzed by Lamm equation modeling using the SEDFIT software of Schuck (58). Positions of menisci and bottoms as well as frictional ratios were optimized during the fitting procedure. The final accepted fits had a root mean square deviation less than 0.006. To obtain information about the amount of oligomers present in samples, absorption and interference data were analyzed globally with SEDPHAT using the hybrid model. In this procedure, monomer, and dimer were fitted as global discrete species with fixed molecular weights and higher molecular weight species were modeled with a continuous sedimentation coefficient distribution.

RESULTS

Sequence Alignment Reveals Conserved Region at the N Terminus of Helix α1—The three-dimensional structure-based sequence alignment between HIV-1-CA and EIAV-CA was performed on individual domains (Fig. 1*A*). The backbone heavy atom root mean square deviation between the two lentiviral CAs are 2.3 Å and 1.4 Å for domains CA^N and CA^C, respectively. Both proteins share 29 and 57% sequence identity

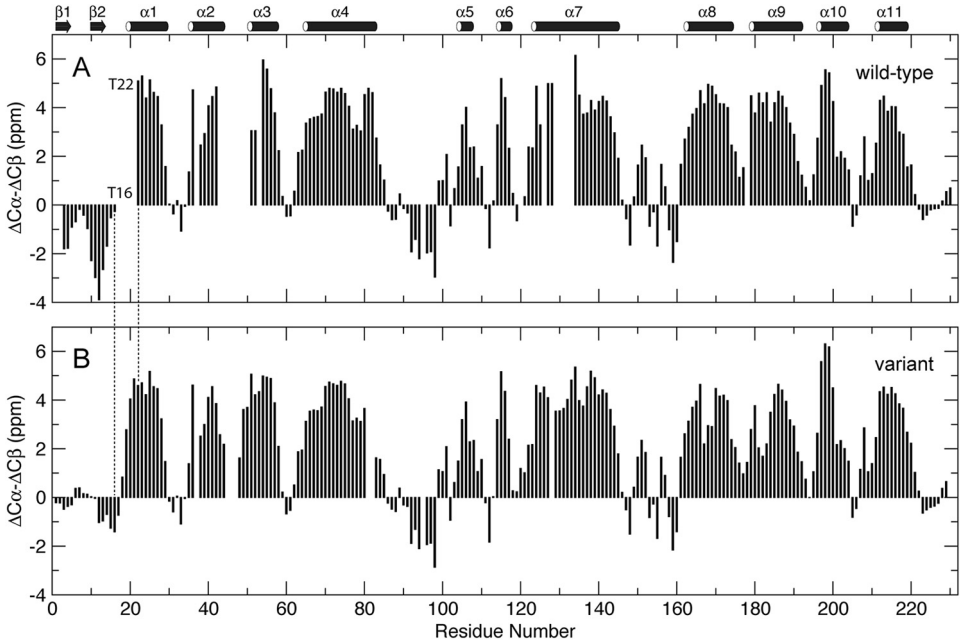

FIGURE 2. **The Cα/β secondary chemical shift indexes of wt (*A*) and variant (*B*) EIAV-CA at pH 6.7.** ΔCα or ΔCβ was the difference between the measured ^{13}C chemical shifts and the values for the same amino acid in the unfolded state (59). The ΔCα-ΔCβ value at residue *i* was the average of the values at residues *i*-1, *i*, and *i*+1 (79).

and homology, respectively. The interesting conserved region is Thr[16]-Pro[17]-Arg[18], corresponding to Ser[16]-Pro[17]-Arg[18] in HIV-1-CA (Fig. 1*A*), where we identified a conformational transition upon folding its upstream β-hairpin motif in the following NMR studies.

Folding the β-Hairpin Extends Helix α1 at Its N Terminus—The protein carbon chemical shifts are sensitive to its local secondary structures (59). NMR resonance assignments were performed on $^{2}H/^{13}C/^{15}N$-labeled wt EIAV-CA protein. At pH 6.7 a total of 186 backbone ^{1}H-^{15}N resonances were assigned, representing 88% of 212 non-proline residues. Residues Ile[2]-Met[3], Arg[18]-Thr[22], Ile[43]-Glu[51], Met[53], Asn[54], Gly[65], Gln[127], and Tyr[129]-Ile[134] (Fig. 1*B*), could not be assigned due to microsecond-millisecond exchange broadening (60) on their ^{1}H-^{15}N resonances. The strong negative Cα/β secondary chemical shift indexes (ΔCα-ΔCβ ≈ −2 ppm) demonstrated the folding of the two N-terminal β-strands (Fig. 2*A*). All prolines, including Pro[90] corresponding to the cyclophilin A binding site on HIV-1-CA (23, 61), were in *trans* conformations according to their Cα/β chemical shifts (62). The Cβ chemical shifts of residues Cys[198] and Cys[218] were over 35 ppm, indicating that the two cysteines form disulfide bridges, consistent with observations reported for HIV-1-CA (63).

The variant protein carrying an N-terminal histidine tag was studied in parallel. Backbone resonances for nearly all of the non-proline residues, except Val[46], Asp[47], and Cys[48], were assigned. The weak Cα/β secondary chemical shift indexes for residues Pro[1]-Arg[18] ($|\Delta C\alpha-\Delta C\beta| < 1.5$ ppm) demonstrated the unfolding of the β-hairpin and N terminus of helix α1 (Fig. 2*B*).

Protein Cα chemical shift (δCα) is positively correlated to the content of its helical structure (59). A comparison of δCα between the wt and variant CA^{N} domains suggested that residues Thr[16] and Thr[22] adopted helix N-capping (64) and helical conformations, respectively (Fig. 3*A* and Table 1). Residues between Thr[16] and Thr[22] in the wt CA have ^{1}H-^{15}N resonances line broadening at pH 6.7, hence no δCα measurements. We lowered the pH to 5.2 to reduce line broadening due to any microsecond-millisecond exchange, and assigned additional ^{1}H-^{15}N resonances for Arg[18], Gly[19], and Thr[21]. The comparison between δCα of the wt at pH 5.2 and the variant (Fig. 3*B*) clearly showed the higher helical content for residues Pro[17], Arg[18], and Gly[19] within the wt EIAV-CA. Normally an α-helix structure features a stretch of successive strong positive (>1 ppm) secondary Cα chemical shifts (ΔCα). Shown in Table 1 are the ΔCα of residues from Leu[15] to Thr[22], which showed that helix α1 starts at Pro[17] and Tyr[20] for the wt and variant EIAV-CA, respectively, and overall the wt has a larger ΔCα value, meaning more stable helical structure. In addition, the program TALOS+ (57) predicted the wt Thr[16] dihedral angles Φ and Ψ to be $-91 \pm 43°$ and $147.5 \pm 29.5°$, respectively, which were close to the typical values predicted for helix N-capping residues, $-94 \pm 15°$ for Φ and $167 \pm 5°$ for Ψ (65). The wt EIAV-CA therefore has Thr[16] to cap helix α1 that starts at Pro[17].

The N-terminal extension of helix α1 can be visualized by aligning crystal structures of the native HIV-1-CA^{N} (23) and the (Pro[1]-Met[3])-deletion mutant of EIAV-CA^{N} (44) (Fig. 3*C*). The Pro[1]-Asp[51] salt bridge stabilizes the β-hairpin motif, which in turn stabilizes and extends helix α1 from Tyr[20] to Pro[17].

Oligomeric Interfaces Include the Extended Helix α1—For HIV-1-CA only at pH values slightly above its pI of 6.6 (17, 66) it could assemble to a mature-like capsid particle (19). In line with such observations we have performed most solution NMR measurements on EIAV-CA at pH 6.7, above its pI value of 6.4, to maximize chances in observing EIAV-CA oligomerization using ^{1}H-^{15}N chemical shift mapping.

For both the wt and variant EIAV-CA high resolution TROSY ^{1}H-^{15}N spectra were collected at pH 6.7 and concentrations of 0.05 and 0.2 mM. If no oligomerization is present

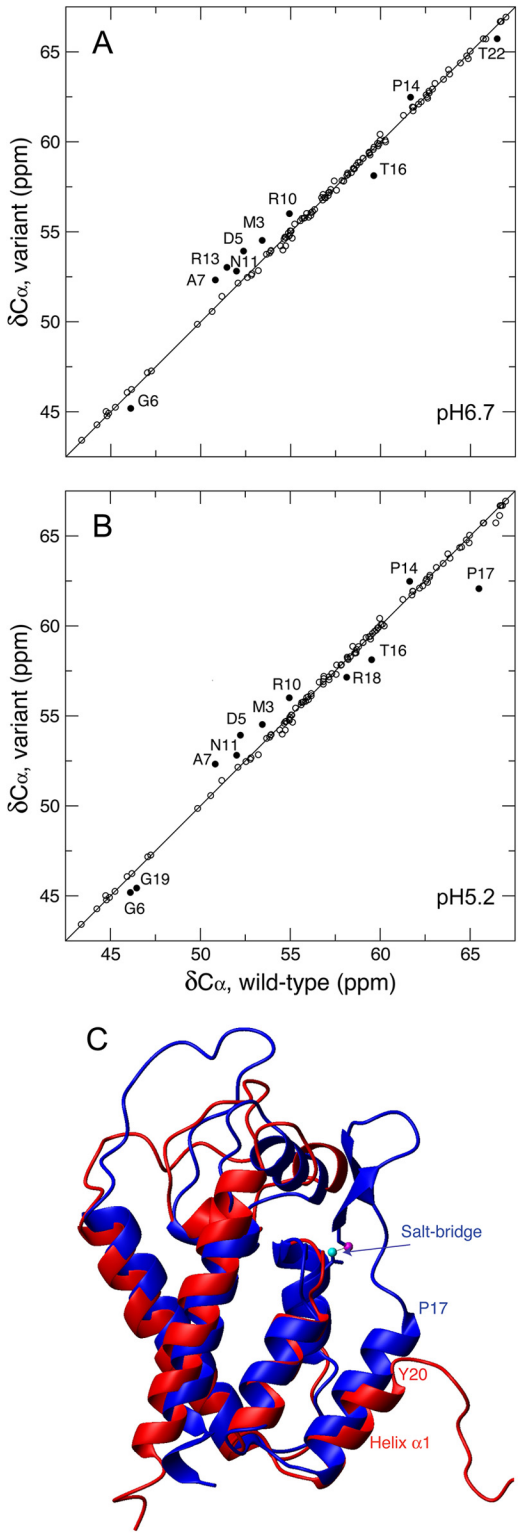

FIGURE 3. **The N-terminal extension of helix α1 based on Cα chemical shifts (δCα).** The δCα correlations between the wt and variant EIAV-CA^N were shown with δCα values of the wt EIAV-CA measured at pH 6.7 (*A*) and 5.2 (*B*). Residues with significant δCα differences (> mean + 1.5 S.D. or < mean − 1.5 S.D.) between the wt and variant are indicated (*A* and *B*). *C*, the overlay of the three-dimensional crystal structures of native HIV-1-CA^N (PDB code 1AK4, *blue*) domain and the (Pro^1-Met^3)-deletion mutant EIAV-CA^N domain (PDB ID 2EIA, *red*). The salt bridge of HIV-1-CA^N involving the nitrogen atom of Pro^1 and one side chain oxygen atom of Asp^{51} were shown in *magenta* and *cyan balls*, respectively. The difference in the N-terminal residue of helix α1 was indicated.

TABLE 1
Secondary ^{13}Cα chemical shift values (ΔCα,defined in the legend to Fig. 2) of helix α1 N-terminal residues

Residue	Wild-type ΔCα pH 6.7[a,b]	Wild-type ΔCα pH 5.2[a,b]	Variant ΔCα, pH 6.7[a,b]
	ppm		*ppm*
Leu^{15}	−0.01 (55.09)	0.02 (55.12)	−0.45 (54.65)
Thr^{16}	−2.48 (59.62)	−2.47 (59.63)	−3.98 (58.12)
Pro^{17}	NA[c]	2.39 (65.49)	−1.03 (62.07)
Arg^{18}	NA	2.04 (58.14)	1.05 (57.15)
Gly^{19}	NA	1.36 (46.46)	0.34 (45.44)
Tyr^{20}	NA	NA	3.74 (61.84)
Thr^{21}	NA	4.54 (66.64)	4.03 (66.13)
Thr^{22}	4.39 (66.49)	4.33 (66.43)	3.63 (65.73)

[a] Shown in the parentheses are the measured chemical shift values of nuclei ^{13}Cα.
[b] Missing chemical shift values were due to ^{1}H-^{15}N line broadening that prohibited ^{13}Cα assignments.
[c] NA, not applicable.

there should not be any changes in the NMR chemical shifts as a function of protein concentration. Those residues that do show large chemical shift changes most likely will be located in the oligomeric interface. Chemical shift changes in backbone ^{1}H-^{15}N resonances (Δ_{N-H}) were normalized and from that a total of four possible oligomeric interfaces were identified (Fig. 4). The wt and variant proteins had nearly identical perturbation profiles for domain CA^C, which clustered around the two interfaces, the domain linker, *e.g.* Asn^{152}, and helix α9, *i.e.* Ile^{181} and Thr^{188}. Thus folding the β-hairpin did not affect oligomerization of domain CA^C, and such oligomerization is in fast nanosecond-microsecond exchange kinetics.

The other two interfaces on domain CA^N were similar between the wt and variant proteins in loci but different in boundaries when the un-assigned exchange-broadened residues were taken into account. Specifically the variant EIAV-CA showed strong chemical shift perturbation around Thr^{21}, close to the N terminus of its helix α1 (Tyr^{20}) (Fig. 4*B*); in comparison, wt EIAV-CA showed chemical shift changes and severe line broadening for residues ranging from its helix α1 capping residue Thr^{16} up to Trp^{23} (Fig. 4*A*) in the middle of the helix. This interface boundary distinction is correlated to the difference in N termini of helix α1, Pro^{17} *versus* Tyr^{20} in the wt and variant proteins, respectively (Table 1). It is conceivable that only helical residues could participate in the oligomeric interface along helix α1. The other CA^N interface is the region spanning helices α2 and α3. Residue Leu^{40}, in the middle of helix α2, was readily identified in chemical shift perturbation for both the wt and variant proteins. For the variant residue Leu^{44} and its neighboring exchange, broadened residues Val^{46}-Cys^{48} were interface residues (Fig. 4*B*). For the wt the exchange broadening was expanded up to Asn^{54} (Fig. 4*A*), in the middle of helix α3. Overall folding of the β-hairpin expanded the domain CA^N oligomeric interfaces in helices α1–3 and caused slower exchange kinetics for interface residues, including those that are too severely broadened to be observed (Fig. 4 and supplemental Fig. S1). The ^{1}H-^{15}N exchange broadening in domain CA^N (supplemental Fig. S1) caused by microsecond-millisecond kinetics usually reflects the existence of sparsely populated excited states potentially carrying biological interests (60, 67, 68), *e.g.* the protein folding and unfolding in populations as small as 1% (69). Formation of the N-terminal β-hairpin has

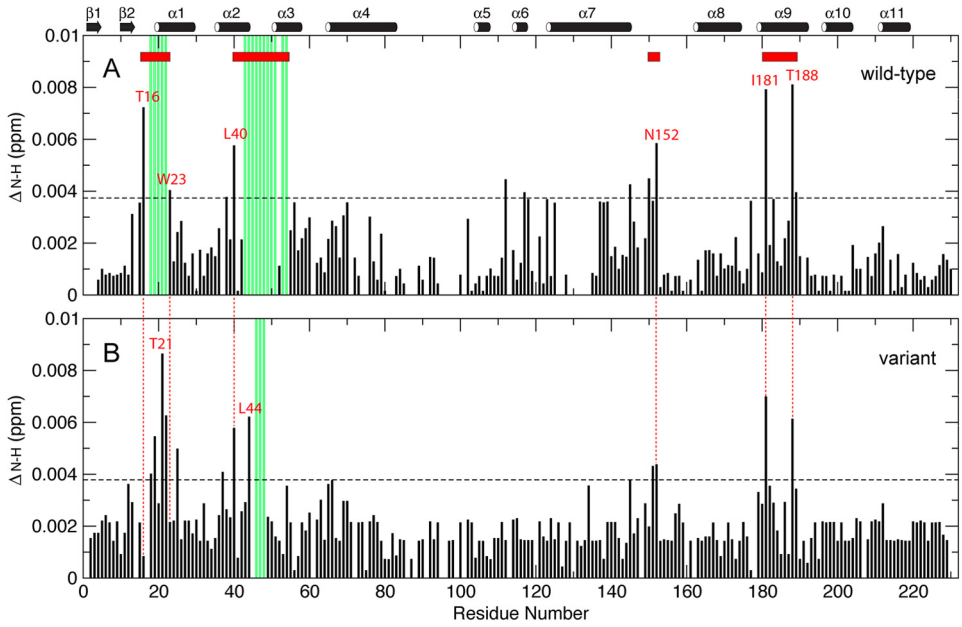

FIGURE 4. **The concentration-dependent backbone ^{15}N-^{1}H resonances chemical shift mapping of wt (*A*) and variant (*B*) EIAV-CA.** The Δ_{NH} value was calculated as the square root of $[\Delta_H^2 + (\Delta_N/5)^2]/2$ (80), where Δ_H and Δ_N were chemical shift differences of ^{1}H and ^{15}N, respectively, taken from the two high resolution TROSY-HSQC spectra collected on 0.2 and 0.05 mM samples for both proteins. The *horizontal dashed line* marks the Δ_{NH} threshold value (mean + 1.5 S.D.). The *red horizontal bars* are the oligomeric interfaces identified in this study based on ^{1}H and ^{15}N chemical shift mapping and severe exchange broadening that prohibits assignment (*green vertical bars*).

been shown to stabilize the structure of the CA^{N} domain (70). Therefore, increased line broadening in the presence of the β-hairpin is less likely due to intramolecular processes. It is also worth noting that the pH change from 6.7 to 5.2 did not alter the Cα chemical shifts for the wt EIAV-CA in the region, *e.g.* Leu^{15}, Thr^{16}, and Thr^{22} (Table 1), which indicated that the microsecond-millisecond exchange broadening at pH 6.7 for ^{1}H-^{15}N resonances was not due to any local structural variations, but to changes in solvent exposure or packing contact due to a shift in the oligomerization equilibrium.

The Monomer-Oligomer Equilibrium—Because the chemical shift mapping and resonance line broadening suggested the presence of both CA^{N}- and CA^{C}-mediated oligomerization at pH 6.7, it would be ideal to cross-validate such oligomers at this pH. The sedimentation velocity profiles of the wt EIAV-CA at pH 4, 6, and 8 all showed one major monomeric species that banded at 2.4 S. A secondary peak at 3.5 S, corresponding to the dimer species, was observed at pH 6 (Fig. 5). An incomplete separation of the dimer peak at pH 4, between 2.5 and 3.0 S, suggested fast dissociation and instability of the dimer. The partial CA dimerization is common among retroviral CAs except for the CAs from primate lentiviruses such as HIV-1 that fully dimerize in solution.

The EIAV-CA^{N} driven oligomer was not detected in analytical ultracentrifugation experiments due to its sparse population, below the general 2% detection limit of analytical ultracentrifugation measurement. Similarly for HIV-1-CA in solution, only the cross-linking method, not sedimentation, could identify oligomers larger than a dimer (17). In fact all crystal structures of CA^{N}-oligomerized HIV-1-CA were obtained on mutants or specially treated proteins that favor oligomerization (39).

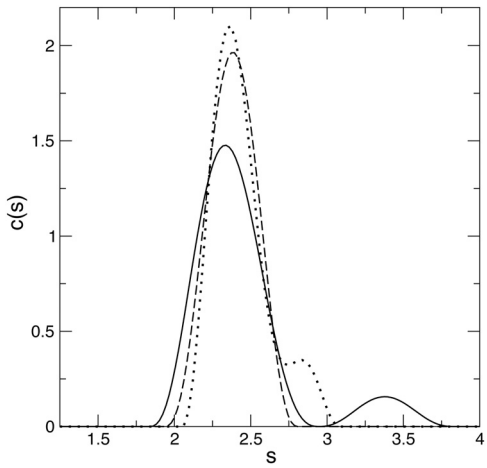

FIGURE 5. **The hydrodynamic results from analytical ultracentrifugation on wt EIAV-CA.** Sedimentation coefficient distributions c(*s*) from the analysis of the sedimentation profiles at pH 4 (*dotted line*), 6 (*solid line*), and 8 (*dashed line*).

Folding of the β-Hairpin Induces Different Domain Alignment and Oligomerization—For solution NMR studies it is important to validate the overall consistency between protein solution and crystal structures by fitting NMR-measured RDCs to existing crystal structure coordinates (71, 72). A total of 150 resolvable backbone ^{1}H-^{15}N RDCs ($D_{N\text{-}H}$) were measured on a 0.15 mM wt sample at pH 6.7. RDC fittings were performed on the individual domains instead. For the CA^{N} and CA^{C} domains, reasonable agreements were obtained, as indicated by *Q* factors of 31 and 22%, respectively, using the coordinates of chain B in the crystal structure (44) (Table 2 and Fig. 6). Because the crystal structure missed the β-hairpin, refinement of the backbone structure coordinates for domain CA^{N} was carried out using XPLOR-NIH (55). After

TABLE 2
The domain specific alignment tensors derived from backbone amide ^{1}H-^{15}N RDCs measured on both the wild-type and the variant EIAV-CA

Protein	Domain	D_a	R	α (°)	β (°)	γ (°)	Q^a
		Hz					
Wild-type	CA^{Nb}	−19.6	0.081	25.0	126	136	31.0%
	CA^{Nc}	−20.5	0.0154	38.2	118	14.8	11.6%
	CA^{Cb}	4.71	0.397	64.1	18.7	37	21.9%
Variant	CA^{Nb}	−17.2	0.320	25.0	117	124	40.8%
	CA^{Cb}	−10.8	0.460	174	79.4	97.5	27.5%

[a] The *Q* factor was calculated according to the published method (76).
[b] The molecular coordinates were from chain b of the EIAV-CA crystal structure (PDB code 2EIA) (44).
[c] The molecular coordinates were from the backbone structure refinement.

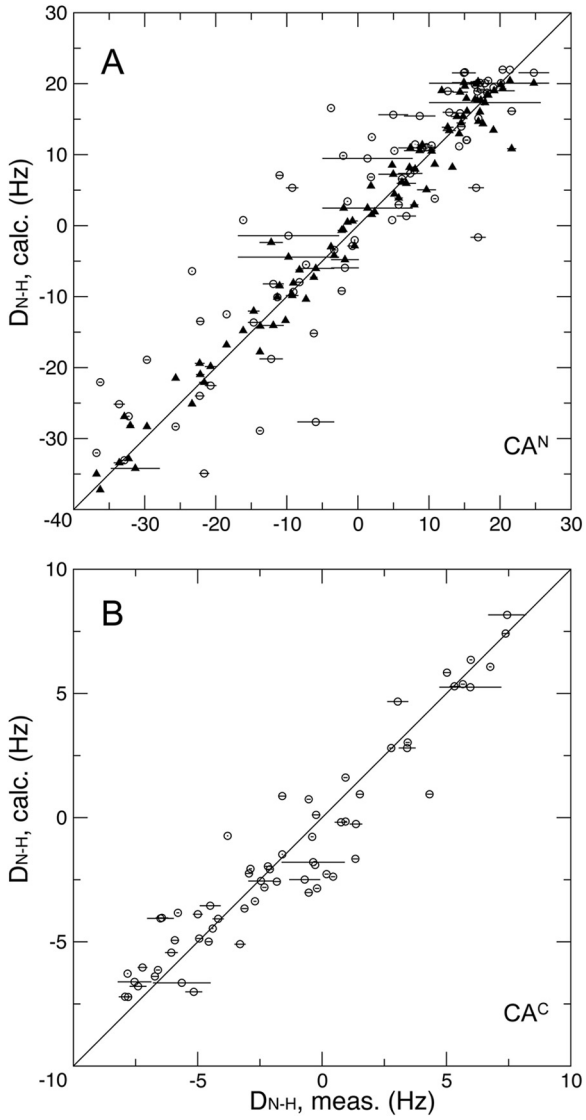

FIGURE 6. **The correlation between the measured backbone ^{1}H-^{15}N RDCs and calculated values for domains CA^N (*A*) and CA^C (*B*) of the wt EIAV-CA at pH 6.7.** The *circles* are fits using the crystal structure coordinate. The *triangles* are the fits using the refined CA^N domain coordinates.

this further refinement, the *Q* factor for the CA^N dropped to 12% (Table 2 and Fig. 6).

In addition to validating the domain structure, the $D_{N\text{-}H}$ determined alignment tensors could qualitatively report inter-domain motion and domain oligomerization. Larger oligomers, ready to be aligned, contribute more into the observed tensor order (D_a) and rhombicity (R). The presence of inter-domain motions would introduce a difference in D_a and R between the two domains. The wt EIAV-CA exhibited the opposite signs of D_a with a difference of −4.4-fold and R difference of 0.38 (theoretical maximum value of R is 0.67) between CA^N and CA^C domains (Table 2), which demonstrated that individual domains participated in two different oligomers that involve significant changes in inter-domain orientation. Measurements on the EIAV-CA variant showed the alignment orders were in the same negative sign with a difference of only 1.6-fold, roughly scale with their size ratio, and a rhombicity R difference of 0.14 (Table 2), both differences were much smaller than the wt values, which indicated the oligomerization within the variant monomer-oligomer equilibriums did not change the inter-domain orientation significantly. Based on the ^{1}H-^{15}N chemical shift mapping profiles (Fig. 4) the CA^C driven oligomerizations were nearly identical for both the wt and variant. Therefore the CA^N oligomerization difference should be the dominant cause for domain tensor parameter differences. The close to zero rhombicity of the wt domain CA^N suggest the presence of CA^N-driven symmetric oligomers, whereas the variant CA^N domain oligomer lacks symmetry with a medium value for rhombicity of 0.32, indicating less CA^N oligomers were formed in the absence of the β-hairpin. This is consistent with the more exchange-broadened residues in the wt CA^N oligomeric interfaces (Fig. 4 and supplemental Fig. S1).

DISCUSSION

Here we have studied the EIAV-CA protein, the first lentiviral CA protein characterized using solution NMR in its native full-length sequence. The NMR data suggested a mechanism for the initial EIAV-CA assembly in solution, *i.e.* upon Gag processing by viral PR, the folding of the β-hairpin structure extends the N terminus of helix α1, the highly conserved Thr/Ser^{16}-Pro^{17}-Arg^{18}, where the CA core assembly initiates. Such a core interface is within a sparse population of the slower forming domain CA^N driven oligomer. The conclusion derived from our NMR results is consistent with previously published data.

Cross-validations on Enhanced/Extended Helix α1 Upon Folding of the β-Hairpin—Our ^{13}Cα chemical shift definitions of the N terminus of helix α1 of EIAV-CA in solution were in line with the published crystallography results. Specifically the crystal structure of the HIV-1-CA^N domain (23) with the β-hairpin have helix α1 starting from residue Pro^{17} and the side chain of Ser^{16} forming a hydrogen bond with the amide of Thr^{19} to cap helix α1. In contrast, the crystal structure of the (Pro^{1}-Met^{3})-deletion mutant EIAV-CA (44), which is missing the β-hairpin, has a shorter helix α1 starting at Tyr^{20}, not Pro^{17} (Fig. 3*C*).

Recent hydrogen-deuterium exchange mass spectrometry identified stronger protection in HIV-1-CA helices α1–3 in the presence of the β-hairpin and suggested helix α1 could be re-oriented upon maturation (73). Stronger protection is consistent with the enhanced helix stability.

Extended Helix α1 Constitutes the Essential CA Assembly Core—Early studies of HIV-1-CA assembly suggested that refolding of the β-hairpin created a new CA-CA interface com-

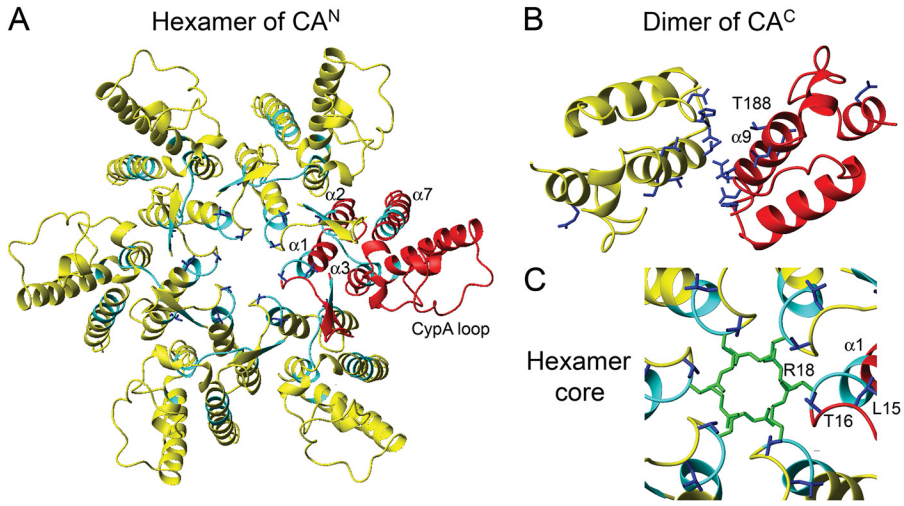

FIGURE 7. **Models for hexameric (*A* and *C*) and dimeric (*B*) interfaces of EIAV-CA.** The side chain bonds of chemical shift mapped residues were colored *blue* in both hexamer (*A*) and dimer (*B*) models, which were generated using rigid body rotation of the refined EIAV-CA^N and the original EIAV-CA^C crystal coordinates onto the crystal structure of HIV-1-CA hexamer (PDB code 3GV2)(39) and the solution structure of HIV-1-CA^C dimer (PDB code 2KOD)(41), respectively. One EIAV-CA molecule was colored *red* in both oligomer models. The *cyan* colored ribbons correspond to residues with severe ^{1}H-^{15}N line broadening. *C*, a close view of the hexamer core. The side chain bonds of the most-inner core residue Arg^{18} were colored *green*.

petent for hexamer formation (2, 74). One hypothesis was that residue Pro^{17} forms the new interface (74). Recently a total of three HIV-1-CA assembly interfaces were identified (38), which are helices α1–3, formed a 18-helix bundle of the CA^N hexamer core, the CA^C dimerization along helix α9, and the inter-molecular and inter-domain contact between helices α4 of the CA^N and α10 of the neighboring CA^C. Among them residue Arg^{18} of helix α1 was located in the deepest center core of the HIV-1-CA hexamer interface (Fig. 7*A*). Arg^{18} is a determinant in HIV-1-CA hexamerization (45), *e.g.* the R18L mutant increases the hexamer population for crystallization (38). All the above evidences from HIV-1-CA are completely in line with our EIAV-CA NMR data showing an expanded oligomeric interface from Thr^{21} to Thr^{16} upon folding of the β-hairpin, incorporating the highly conserved and newly formed helical sequence of Pro^{17}-Arg^{18}-Gly^{19}.

In addition to identifying the β-hairpin induced structural effects, our NMR data suggested the two CA domains independently drive oligomerization, *i.e.* the readily formed domain CA^C dimerization along helix α9 (Fig. 7*B*) is in fast kinetics (supplemental Fig. S1), in contrast, the domain CA^N has to structure the helix α1 to position the side chain of its Arg^{18} toward the inner core of the hexamer (Fig. 7*C*), overcoming a repulsion energy barrier and thus kinetically slower (supplemental Fig. S1). Therefore it is not surprising that the CA^N-driven oligomer at the experimental sub-millimolar concentration was a sparse population (probably <1%). However, the CA assembly could still be efficient within a retrovirion where the CA concentration is much higher (75).

Acknowledgments—We thank Charles Schwieters for professional help with XPOLR-NIH, Motoshi Suzuki for help with the sample preparation, Duck-Yeon Lee for expertise regarding mass spectrometry, and Alex Grishaev and Yaroslav Ryabov for helpful suggestions.

REFERENCES

1. Strauss, J. H., and Strauss, E. G. (2008) *Viruses and Human Disease*, 2nd Ed., Elsevier/Academic Press, Amsterdam
2. von Schwedler, U. K., Stemmler, T. L., Klishko, V. Y., Li, S., Albertine, K. H., Davis, D. R., and Sundquist, W. I. (1998) Proteolytic refolding of the HIV-1 capsid protein amino-terminus facilitates viral core assembly. *EMBO J.* **17,** 1555–1568
3. Gross, I., Hohenberg, H., Huckhagel, C., and Kräusslich, H. G. (1998) N-Terminal extension of human immunodeficiency virus capsid protein converts the *in vitro* assembly phenotype from tubular to spherical particles. *J. Virol.* **72,** 4798–4810
4. Rayne, F., Bouamr, F., Lalanne, J., and Mamoun, R. Z. (2001) The NH_2-terminal domain of the human T-cell leukemia virus type 1 capsid protein is involved in particle formation. *J. Virol.* **75,** 5277–5287
5. Nandhagopal, N., Simpson, A. A., Johnson, M. C., Francisco, A. B., Schatz, G. W., Rossmann, M. G., and Vogt, V. M. (2004) Dimeric Rous sarcoma virus capsid protein structure relevant to immature Gag assembly. *J. Mol. Biol.* **335,** 275–282
6. Wildová, M., Hadravová, R., Stokrová, J., Krízová, I., Ruml, T., Hunter, E., Pichová, I., and Rumlová, M. (2008) The effect of point mutations within the N-terminal domain of Mason-Pfizer monkey virus capsid protein on virus core assembly and infectivity. *Virology* **380,** 157–163
7. von Schwedler, U. K., Stray, K. M., Garrus, J. E., and Sundquist, W. I. (2003) Functional surfaces of the human immunodeficiency virus type 1 capsid protein. *J. Virol.* **77,** 5439–5450
8. Purdy, J. G., Flanagan, J. M., Ropson, I. J., Rennoll-Bankert, K. E., and Craven, R. C. (2008) Critical role of conserved hydrophobic residues within the major homology region in mature retroviral capsid assembly. *J. Virol.* **82,** 5951–5961
9. Wills, J. W., and Craven, R. C. (1991) Form, function, and use of retroviral gag proteins. *Aids* **5,** 639–654
10. Scarlata, S., and Carter, C. (2003) Role of HIV-1 Gag domains in viral assembly. *Biochim. Biophys. Acta* **1614,** 62–72
11. Carter, C. A., and Ehrlich, L. S. (2008) Cell biology of HIV-1 infection of macrophages. *Annu. Rev. Microbiol.* **62,** 425–443
12. Roberts, M. M., and Oroszlan, S. (1989) The preparation and biochemical characterization of intact capsids of equine infectious anemia virus. *Biochem. Biophys. Res. Commun.* **160,** 486–494
13. Stephens, R. M., Casey, J. W., and Rice, N. R. (1986) Equine infectious anemia virus *gag* and *pol* genes. Relatedness to visna and AIDS virus. *Science* **231,** 589–594
14. Gelderblom, H. R. (1991) Assembly and morphology of HIV: potential

effect of structure on viral function. *AIDS* **5,** 617–637
15. Cairns, T. M., and Craven, R. C. (2001) Viral DNA synthesis defects in assembly-competent Rous sarcoma virus CA mutants. *J. Virol.* **75,** 242–250
16. Roa, A., Hayashi, F., Yang, Y., Lienlaf, M., Zhou, J., Shi, J., Watanabe, S., Kigawa, T., Yokoyama, S., Aiken, C., and Diaz-Griffero, F. (2012) RING domain mutations uncouple TRIM5α restriction of HIV-1 from inhibition of reverse transcription and acceleration of uncoating. *J. Virol.* **86,** 1717–1727
17. Ehrlich, L. S., Agresta, B. E., and Carter, C. A. (1992) Assembly of recombinant human immunodeficiency virus type 1 capsid protein in vitro. *J. Virol.* **66,** 4874–4883
18. Rosé, S., Hensley, P., O'Shannessy, D. J., Culp, J., Debouck, C., and Chaiken, I. (1992) Characterization of HIV-1 p24 self-association using analytical affinity chromatography. *Proteins Struct. Funct. Genet.* **13,** 112–119
19. Ehrlich, L. S., Liu, T., Scarlata, S., Chu, B., and Carter, C. A. (2001) HIV-1 capsid protein forms spherical (immature-like) and tubular (mature-like) particles *in vitro*. Structure switching by pH-induced conformational changes. *Biophys. J.* **81,** 586–594
20. Campbell, S., and Vogt, V. M. (1995) Self-assembly *in vitro* of purified CA-NC proteins from Rous sarcoma virus and human immunodeficiency virus type 1. *J. Virol.* **69,** 6487–6497
21. Gross, I., Hohenberg, H., and Kräusslich, H. G. (1997) *In vitro* assembly properties of purified bacterially expressed capsid proteins of human immunodeficiency virus. *Eur. J. Biochem.* **249,** 592–600
22. Gitti, R. K., Lee, B. M., Walker, J., Summers, M. F., Yoo, S., and Sundquist, W. I. (1996) Structure of the amino-terminal core domain of the HIV-1 capsid protein. *Science* **273,** 231–235
23. Gamble, T. R., Vajdos, F. F., Yoo, S., Worthylake, D. K., Houseweart, M., Sundquist, W. I., and Hill, C. P. (1996) Crystal structure of human cyclophilin A bound to the amino-terminal domain of HIV-1 capsid. *Cell* **87,** 1285–1294
24. Momany, C., Kovari, L. C., Prongay, A. J., Keller, W., Gitti, R. K., Lee, B. M., Gorbalenya, A. E., Tong, L., McClure, J., Ehrlich, L. S., Summers, M. F., Carter, C., and Rossmann, M. G. (1996) Crystal structure of dimeric HIV-1 capsid protein. *Nat. Struct. Biol.* **3,** 763–770
25. Gamble, T. R., Yoo, S., Vajdos, F. F., von Schwedler, U. K., Worthylake, D. K., Wang, H., McCutcheon, J. P., Sundquist, W. I., and Hill, C. P. (1997) Structure of the carboxyl-terminal dimerization domain of the HIV-1 capsid protein. *Science* **278,** 849–853
26. Cornilescu, C. C., Bouamr, F., Yao, X., Carter, C., and Tjandra, N. (2001) Structural analysis of the N-terminal domain of the human T-cell leukemia virus capsid protein. *J. Mol. Biol.* **306,** 783–797
27. Tang, C., Ndassa, Y., and Summers, M. F. (2002) Structure of the N-terminal 283-residue fragment of the immature HIV-1 Gag polyprotein. *Nat. Struct. Biol.* **9,** 537–543
28. Macek, P., Chmelík, J., Krízová, I., Kaderávek, P., Padrta, P., Zídek, L., Wildová, M., Hadravová, R., Chaloupková, R., Pichová, I., Ruml, T., Rumlová, M., and Sklenár, V. (2009) NMR structure of the N-terminal domain of capsid protein from the Mason-Pfizer monkey virus. *J. Mol. Biol.* **392,** 100–114
29. Yoo, S., Myszka, D. G., Yeh, C., McMurray, M., Hill, C. P., and Sundquist, W. I. (1997) Molecular recognition in the HIV-1 capsid/cyclophilin A complex. *J. Mol. Biol.* **269,** 780–795
30. Berthet-Colominas, C., Monaco, S., Novelli, A., Sibaï, G., Mallet, F., and Cusack, S. (1999) Head-to-tail dimers and interdomain flexibility revealed by the crystal structure of HIV-1 capsid protein (p24) complexed with a monoclonal antibody Fab. *EMBO J.* **18,** 1124–1136
31. Khorasanizadeh, S., Campos-Olivas, R., and Summers, M. F. (1999) Solution structure of the capsid protein from the human T-cell leukemia virus type-I. *J. Mol. Biol.* **291,** 491–505
32. Campos-Olivas, R., Newman, J. L., and Summers, M. F. (2000) Solution structure and dynamics of the Rous sarcoma virus capsid protein and comparison with capsid proteins of other retroviruses. *J. Mol. Biol.* **296,** 633–649
33. Du, S., Betts, L., Yang, R., Shi, H., Concel, J., Ahn, J., Aiken, C., Zhang, P., and Yeh, J. I. (2011) Structure of the HIV-1 full-length capsid protein in a conformationally trapped unassembled state induced by small-molecule binding. *J. Mol. Biol.* **406,** 371–386
34. Turner, B. G., and Summers, M. F. (1999) Structural biology of HIV. *J. Mol. Biol.* **285,** 1–32
35. Ganser, B. K., Li, S., Klishko, V. Y., Finch, J. T., and Sundquist, W. I. (1999) Assembly and analysis of conical models for the HIV-1 core. *Science* **283,** 80–83
36. Briggs, J. A., Wilk, T., Welker, R., Kräusslich, H. G., and Fuller, S. D. (2003) Structural organization of authentic, mature HIV-1 virions and cores. *EMBO J.* **22,** 1707–1715
37. Mortuza, G. B., Haire, L. F., Stevens, A., Smerdon, S. J., Stoye, J. P., and Taylor, I. A. (2004) High-resolution structure of a retroviral capsid hexameric amino-terminal domain. *Nature* **431,** 481–485
38. Ganser-Pornillos, B. K., Cheng, A., and Yeager, M. (2007) Structure of full-length HIV-1 CA. A model for the mature capsid lattice. *Cell* **131,** 70–79
39. Pornillos, O., Ganser-Pornillos, B. K., Kelly, B. N., Hua, Y., Whitby, F. G., Stout, C. D., Sundquist, W. I., Hill, C. P., and Yeager, M. (2009) X-ray structures of the hexameric building block of the HIV capsid. *Cell* **137,** 1282–1292
40. Cardone, G., Purdy, J. G., Cheng, N., Craven, R. C., and Steven, A. C. (2009) Visualization of a missing link in retrovirus capsid assembly. *Nature* **457,** 694–698
41. Byeon, I. J., Meng, X., Jung, J., Zhao, G., Yang, R., Ahn, J., Shi, J., Concel, J., Aiken, C., Zhang, P., and Gronenborn, A. M., (2009) Structural convergence between cryo-EM and NMR reveals intersubunit interactions critical for HIV-1 capsid function. *Cell* **139,** 780–790
42. Pornillos, O., Ganser-Pornillos, B. K., and Yeager, M. (2011) Atomic-level modelling of the HIV capsid. *Nature* **469,** 424–427
43. Langelier, C. R., Sandrin, V., Eckert, D. M., Christensen, D. E., Chandrasekaran, V., Alam, S. L., Aiken, C., Olsen, J. C., Kar, A. K., Sodroski, J. G., and Sundquist, W. I. (2008) Biochemical characterization of a recombinant TRIM5α protein that restricts human immunodeficiency virus type 1 replication. *J. Virol.* **82,** 11682–11694
44. Jin, Z., Jin, L., Peterson, D. L., and Lawson, C. L. (1999) Model for lentivirus capsid core assembly based on crystal dimers of EIAV p26. *J. Mol. Biol.* **286,** 83–93
45. Ganser-Pornillos, B. K., von Schwedler, U. K., Stray, K. M., Aiken, C., and Sundquist, W. I. (2004) Assembly properties of the human immunodeficiency virus type 1 CA protein. *J. Virol.* **78,** 2545–2552
46. López, C. S., Eccles, J. D., Still, A., Sloan, R. E., Barklis, R. L., Tsagli, S. M., and Barklis, E. (2011) Determinants of the HIV-1 core assembly pathway. *Virology* **417,** 137–146
47. Pervushin, K., Riek, R., Wider, G., and Wüthrich, K. (1997) Attenuated T2 relaxation by mutual cancellation of dipole-dipole coupling and chemical shift anisotropy indicates an avenue to NMR structures of very large biological macromolecules in solution. *Proc. Natl. Acad. Sci. U.S.A.* **94,** 12366–12371
48. Rance, M., Loria, J. P., and Palmer, A. G. (1999) Sensitivity improvement of transverse relaxation-optimized spectroscopy. *J. Magn. Reson.* **136,** 92–101
49. Yang, D. W., Venters, R. A., Mueller, G. A., Choy, W. Y., and Kay, L. E. (1999) TROSY-based HNCO pulse sequences for the measurement of (HN)-H^1-N^{15}, N^{15}-(CO)-C^{13}, (HN)-H^1-(CO)-C^{13}, (CO)-C^{13}-$C^{13}(\alpha)$ and (HN)-H^1-$C^{13}(\alpha)$ dipolar couplings in N^{15}, C^{13}, H^2-labeled proteins. *J. Biomol. NMR* **14,** 333–343
50. Yang, D. W., and Kay, L. E. (1999) TROSY triple-resonance four-dimensional NMR spectroscopy of a 46-ns tumbling protein. *J. Am. Chem. Soc.* **121,** 2571–2575
51. Salzmann, M., Wider, G., Pervushin, K., Senn, H., and Wuthrich, K. (1999) TROSY-type triple-resonance experiments for sequential NMR assignments of large proteins. *J. Am. Chem. Soc.* **121,** 844–848
52. Zhu, G., Kong, X. M., and Sze, K. H. (1999) Gradient and sensitivity enhancement of 2D TROSY with water flip-back, 3D NOESY-TROSY and TOCSY-TROSY experiments. *J. Biomol. NMR* **13,** 77–81
53. Delaglio, F., Grzesiek, S., Vuister, G. W., Zhu, G., Pfeifer, J., and Bax, A. (1995) NMRPipe. A multidimensional spectral processing system based on UNIX pipes. *J. Biomol. NMR* **6,** 277–293
54. Hansen, M. R., Mueller, L., and Pardi, A. (1998) Tunable alignment of

macromolecules by filamentous phage yields dipolar coupling interactions. *Nat. Struct. Biol.* **5,** 1065–1074
55. Schwieters, C. D., Kuszewski, J. J., Tjandra, N., and Clore, G. M. (2003) The Xplor-NIH NMR molecular structure determination package. *J. Magn. Reson.* **160,** 65–73
56. Schwieters, C. D., Kuszewski, J. J., and Clore, G. M. (2006) Using Xplor-NIH for NMR molecular structure determination. *Prog. Nucl. Magn. Reson. Spectrosc.* **48,** 47–62
57. Shen, Y., Delaglio, F., Cornilescu, G., and Bax, A. (2009) TALOS$^+$. A hybrid method for predicting protein backbone torsion angles from NMR chemical shifts. *J. Biomol. NMR* **44,** 213–223
58. Schuck, P. (2003) On the analysis of protein self-association by sedimentation velocity analytical ultracentrifugation. *Anal. Biochem.* **320,** 104–124
59. Spera, S., and Bax, A. (1991) Empirical correlation between protein backbone conformation and Cα and Cβ C^{13} nuclear magnetic resonance chemical shifts. *J. Am. Chem. Soc.* **113,** 5490–5492
60. Palmer, A. G., Kroenke, C. D., and Loria, J. P. (2001) Nuclear magnetic resonance methods for quantifying microsecond-to-millisecond motions in biological macromolecules. *Nuclear Magn. Reson. Biol. Macromolecules* **339,** 204–238
61. Bosco, D. A., Eisenmesser, E. Z., Pochapsky, S., Sundquist, W. I., and Kern, D. (2002) Catalysis of *cis*/*trans* isomerization in native HIV-1 capsid by human cyclophilin A. *Proc. Natl. Acad. Sci. U.S.A.* **99,** 5247–5252
62. Shen, Y., and Bax, A. (2010) Prediction of Xaa-Pro peptide bond conformation from sequence and chemical shifts. *J. Biomol. NMR* **46,** 199–204
63. Hausdorf, G., Gewiess, A., Wray, V., and Porstmann, T. (1994) A recombinant human immunodeficiency virus type-1 capsid protein (rp24). Its expression, purification and physico-chemical characterization. *J. Virol. Methods* **50,** 1–9
64. Gronenborn, A. M., and Clore, G. M. (1994) Identification of N-terminal helix capping boxes by means of 13C chemical shifts. *J. Biomol. NMR* **4,** 455–458
65. Harper, E. T., and Rose, G. D. (1993) Helix stop signals in proteins and peptides. The capping box. *Biochemistry* **32,** 7605–7609
66. Laurent, A. G., Krust, B., Rey, M. A., Montagnier, L., and Hovanessian, A. G. (1989) Cell surface expression of several species of human immunodeficiency virus type 1 major core protein. *J. Virol.* **63,** 4074–4078
67. Kern, D., and Zuiderweg, E. R. (2003) The role of dynamics in allosteric regulation. *Curr. Opin. Struct. Biol.* **13,** 748–757
68. Mittermaier, A. K., and Kay, L. E. (2009) Observing biological dynamics at atomic resolution using NMR. *Trends Biochem. Sci.* **34,** 601–611
69. Meinhold, D. W., and Wright, P. E. (2011) Measurement of protein unfolding/refolding kinetics and structural characterization of hidden intermediates by NMR relaxation dispersion. *Proc. Natl. Acad. Sci. U.S.A.* **108,** 9078–9083
70. Bouamr, F., Cornilescu, C. C., Goff, S. P., Tjandra, N., and Carter, C. A. (2005) Structural and dynamics studies of the D54A mutant of human T cell leukemia virus-1 capsid protein. *J. Biol. Chem.* **280,** 6792–6801
71. Tjandra, N., and Bax, A. (1997) Direct measurement of distances and angles in biomolecules by NMR in a dilute liquid crystalline medium. *Science* **278,** 1111–1114
72. Bax, A. (2003) Weak alignment offers new NMR opportunities to study protein structure and dynamics. *Protein Sci.* **12,** 1–16
73. Cortines, J. R., Monroe, E. B., Kang, S., and Prevelige, P. E. (2011) A retroviral chimeric capsid protein reveals the role of the N-terminal β-hairpin in mature core assembly. *J. Mol. Biol.* **410,** 641–652
74. Kelly, B. N., Howard, B. R., Wang, H., Robinson, H., Sundquist, W. I., and Hill, C. P. (2006) Implications for viral capsid assembly from crystal structures of HIV-1 Gag(1–278) and CA(N)(133–278). *Biochemistry* **45,** 11257–11266
75. Briggs, J. A., Simon, M. N., Gross, I., Kräusslich, H. G., Fuller, S. D., Vogt, V. M., and Johnson, M. C. (2004) The stoichiometry of Gag protein in HIV-1. *Nat. Struct. Mol. Biol.* **11,** 672–675
76. Clore, G. M., and Garrett, D. S. (1999) *R*-factor, free *R*, and complete cross-validation for dipolar coupling refinement of NMR structures. *J. Am. Chem. Soc.* **121,** 9008–9012
77. Shindyalov, I. N., and Bourne, P. E. (1998) Protein structure alignment by incremental combinatorial extension (CE) of the optimal path. *Protein Eng.* **11,** 739–747
78. Worthylake, D. K., Wang, H., Yoo, S., Sundquist, W. I., and Hill, C. P. (1999) Structures of the HIV-1 capsid protein dimerization domain at 2.6-Å resolution. *Acta Crystallogr. D Biol. Crystallogr.* **55,** 85–92
79. Metzler, W. J., Constantine, K. L., Friedrichs, M. S., Bell, A. J., Ernst, E. G., Lavoie, T. B., and Mueller, L. (1993) Characterization of the three-dimensional solution structure of human profilin. ^{1}H, ^{13}C, and ^{15}N NMR assignments and global folding pattern. *Biochemistry* **32,** 13818–13829
80. Garrett, D. S., Seok, Y. J., Peterkofsky, A., Clore, G. M., and Gronenborn, A. M. (1997) Identification by NMR of the binding surface for the histidine-containing phosphocarrier protein HPr on the N-terminal domain of enzyme I of the *Escherichia coli* phosphotransferase system. *Biochemistry* **36,** 4393–4398